Chemical Cogeneration in Solid Electrolyte Cells

The Oxidation of H_2S to SO_2

I. V. Yentekakis[1] and C. G. Vayenas*

Institute of Chemical Engineering and High Temperature Chemical Processes, Department of Chemical Engineering, University of Patras, Patras GR 26110, Greece

ABSTRACT

The anodic oxidation of H_2S was investigated in the solid electrolyte fuel cell H_2S, S_x, SO_2, Pt/ZrO_2(8% Y_2O_3)/Pt, air operating at atmospheric pressure and temperatures 650° to 800°C. It was found that the fuel cell product selectivity crucially depends on the ratio M of the fluxes of oxygen anions O^{2-} and H_2S reaching the porous Pt anode. When $M < 0.33$, elemental sulfur is the major product, and the anode is severely polarized. For higher M values, the product selectivity to SO_2 exceeds 99% at H_2S conversions as high as 99%. The cell appears to be a promising candidate for the cogeneration of electric energy and sulfur dioxide.

The oxidation of hydrogen sulfide to sulfur dioxide is one of the basic steps of the Claus process and, ultimately, of the industrial manufacture of sulfuric acid, which ranks first in volume among all chemicals produced with an annual worldwide production exceeding $3 \cdot 10^8$ tons. The conversion of H_2S to SO_2 is a highly exothermic reaction with $\Delta G° = -103.6$ kcal/mole SO_2 at 800°C. Due to the high exothermicity of the reaction, large amounts of thermal energy are generated. It has been a long-sought goal to obtain this energy as electric rather than thermal energy by oxidizing H_2S to SO_2 in a fuel cell (1, 2).

Low-temperature fuel cells are severely polarized by H_2S and sulfur. High-temperature solid electrolyte cells have been tested for years as fuel cells with H_2, CO, or CH_4 as the fuel (3-8). The same type of cells can be used to study the mechanism of catalytic reactions on metals (9-12) and also to influence the activity and selectivity of metal catalysts by electrochemically pumping oxygen anions O^{2-} onto catalyst surfaces (13-17). Progress in this area has been reviewed recently (18). In some very recent studies (17, 19-21) it has been found that the increase in catalytic reaction rate can exceed the rate of O^{2-} pumping to the catalyst by as much as a factor of 10^5 with a concomitant 40-fold increase in catalytic reaction rate over its open-circuit value (19-20). The acronym NEMCA (non-faradaic electrochemical modification of catalytic activity) has been used to describe this new phenomenon which has been attributed to changes induced to the average catalyst work function due to the interaction of the catalyst surface with excess O^{2-} (17, 19-21).

One of the emerging uses of solid electrolyte cells is chemical cogeneration, *i.e.*, the simultaneous production of electrical power and useful chemicals.

This mode of operation combines the concepts of a fuel cell and of a chemical reactor. Its feasibility was first demonstrated in 1980 when it was shown that solid oxide fuel cells with Pt-based electrodes can quantitatively convert NH_3 to NO with simultaneous generation of electrical power (22-24). Subsequent work has shown that four other exothermic reactions of industrial importance can also be carried out successfully in solid oxide fuel cell reactors with appropriate electrocatalytic anodes. These are the oxidative dehydrogenation of ethylbenzene to styrene (25, 26) and 1-butene to butadiene (27), the Adrussov process, *i.e.*, the ammoxidation of methane to form HCN (28) and, more recently, the partial oxidation of methanol to formaldehyde (18, 29). In all these studies, product selectivity was found to depend rather strongly on operating conditions and, in particular, on cell current.

There have been two very recent studies of the anodic oxidation of H_2S in high-temperature yttria-stabilized zirconia cells (30, 31). In one study the thiospinel $CuFe_2S_4$ was used as the anode material. Preliminary results showed that the current-potential curves of the cell were dominated by the ohmic resistance of the electrolyte (30). In the second study (31) the effect of H_2S poisoning on the anodic oxidation of H_2 was investigated on Au, Ni, and Pt anodes. The effect of current on anodic overpotential was studied both on regular and on electrolytically colored yttria stabilized zirconia. The authors found evidence for electrocatalysis by F-centers present on the zirconia (31). No direct information on the cell power output characteristics was given but it was found that the use of electrolytically colored zirconia reduces the anodic overpotential by a factor of ten (31). Unfortunately, no product analysis was performed in these two recent studies and therefore no qualitative or quantitative information is available about the nature of the anodic reactions and about fuel cell product distribution.

In this work, H_2S was used as the fuel in a high-temperature solid electrolyte fuel cell with porous Pt electrodes in order to study the electrochemical characteristics and product distribution of the cell and explore the possibility of simultaneous generation of SO_2 and electrical power.

Experimental Apparatus

A schematic diagram of the experimental apparatus, which has been described in previous communications (9-12, 17, 24), is shown in Fig. 1. It consists of a gas feed system, the fuel cell, and the analytical system. The fuel cell is shown in Fig. 2. It consists of an 8 mole percent (m/o) yttria stabilized zirconia tube closed flat at one end. Porous Pt electrodes were deposited on the inside and outside bottom wall of the stabilized tube using an Engelhard-Hannovia A1121 Pt paste followed by drying and calcination at 850°C for 5h. Electrode preparation and characterization details have appeared elsewhere (12, 17). The porous Pt electrodes were approximately 5 μm thick and contained no measurable metal impurities as shown by XPS (12, 17). A three-electrode system shown in Fig. 2 was used. The superficial surface areas of the anodic, cathodic, and reference electrodes were 2.0, 1.5, and 0.1 cm^2, respectively. A decade resistance box was used to vary cell load. Constant

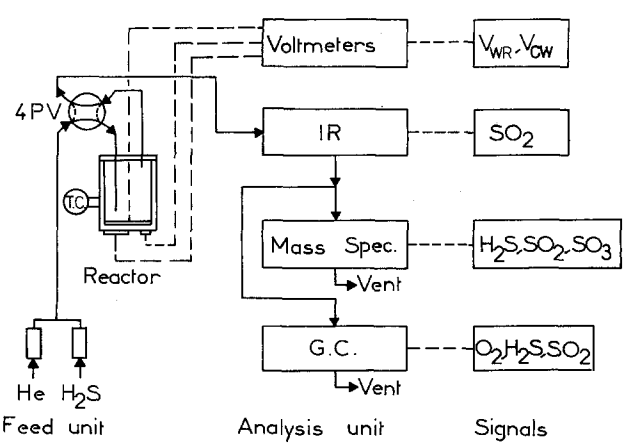

Fig. 1. Schematic diagram of the apparatus

* Electrochemical Society Active Member.

[1] Present address: Department of Chemical Engineering, Princeton University, New Jersey 08544.

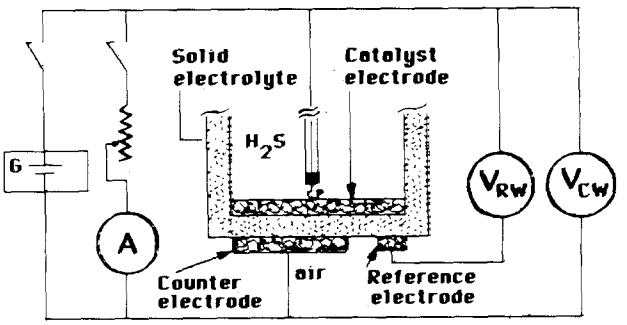

Fig. 2. Fuel cell geometry and electrode configuration

currents or potentials could be applied to the cell, when necessary, using an AMEL 553 galvanostat-potentiostat. The voltage between the anode and the reference electrode was measured by a Fluke 891Å differential voltmeter. Other voltages and currents were measured by Fluke 8600Å digital multimeters.

The open end of the stabilized zirconia tube was clamped to an appropriately machined water-cooled stainless-steel cap which had provisions for introduction of reactants and removal of products through quartz tubes and also for introduction of a Pt wire partly enclosed in a quartz tube to establish contact with the Pt anode.

Reactants were Linde standard H_2S diluted in He which could be further diluted in ultrapure (99.999%) He. The cathodic and reference electrodes were exposed to ambient air.

As shown in Fig. 1, reactants and products were analyzed by three independent techniques:

1. On-line gas chromatography for H_2S, SO_2, and H_2O using a Perkin-Elmer sigma-2 gas chromatograph with a TC detector and a 6 ft Teflon Chromosorb 107 80/100 column.
2. On-line mass spectroscopy using a Balzers QMG311 quadrapole mass spectrometer with a QDP 101 data processor which permitted simultaneous monitoring of the exit concentrations of H_2S, SO_2, SO_3, and H_2O.
3. On-line IR spectroscopy using a Beckman Model 864 nondispersive SO_2 analyzer.

Sulfur produced by the cell at low current densities was not allowed to reach the analysis system by condensing it in the water-cooled reactor cap, which had to be cleaned after long periods of operation.

Results

Close agreement was observed (±0.5%) between measured and theoretical EMF values when O_2, N_2, or He mixtures of known p_{O_2} were fed through the zirconia cell reactor. This verified the pure anionic conductivity of the solid electrolyte.

Figure 3a shows typical results of the cell reactor performance at low current densities, spontaneously generated by the cell. The parameter M, which appears as a second abscissa in Fig. 3 and in subsequent figures plays an important role in cell performance. It is a stoichiometric oxygen-to-fuel ratio defined from

$$M = \frac{I}{6\mathbf{F}G\,y^{\circ}_{H_2S}} \qquad [1]$$

where I is the current, $\mathbf{F}$ is Faraday's constant, G is the total gaseous molar flow rate fed to the anode, and $y^{\circ}_{H_2S}$ is the feed H_2S mole fraction. When $M = 1$, the cell current is exactly that required to completely convert H_2S to SO_2 according to the reaction

$$H_2S + 3\,O^{2-} \rightarrow SO_2 + H_2O + 6e^- \qquad [2]$$

As shown in Fig. 3, which is restricted to low M values, the open-circuit EMF is near 1V, and the rate of H_2S consumption r_{H_2S} does not vanish at open-circuit conditions. This is due to the reaction

$$H_2S \rightarrow H_2 + S \qquad [3]$$

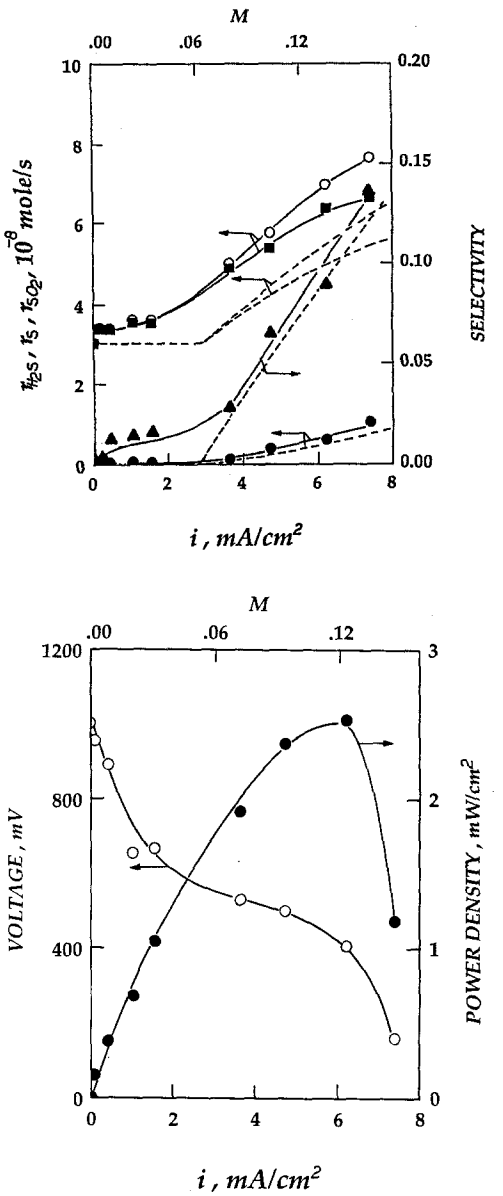

Fig. 3. (a, top) Effect of current density or r_{H_2S} (○), r_S (■), r_{SO_2} (●), and selectivity (▲) at low M values. $G = 3.8 \cdot 10^{-5}$ M/s, $y^{\circ}_{H_2S} = 0.42 \cdot 10^{-2}$, $T = 730$°C, cell-reactor 1. Active electrolyte surface area ≈ 2 cm^2. Dashed curves from model. (b, bottom) Dependence of cell voltage V_{CW} and power density on current density and M. Conditions as in Fig. 3a.

which is catalyzed by the porous Pt electrode. It should be noted that over the temperature range of this investigation, S_2(g) is the dominant gaseous sulfur species. However, to simplify the notation we have used the symbol S instead of 1/2 S_2(g) throughout this paper. As shown in Fig. 3a, increasing current density causes an increase in r_{H_2S} and also in the rate of sulfur formation r_S. There appears to exist a threshold M value (~0.06) in order to obtain a measurable rate of SO_2 formation r_{SO_2}. Subsequent increases in current density and M cause increases in r_{SO_2}. The selectivity to SO_2 defined from

$$s = r_{SO_2}/r_{H_2S} \qquad [4]$$

remains low, typically, below 15%, and the main fuel cell product is sulfur, which is produced by the catalytic reaction [3] and also by the electrocatalytic reaction

$$H_2S + O^{2-} \rightarrow H_2O + S + 2e^- \qquad [5]$$

The observed maxima in the net rate of S production r_S with increasing current shown in subsequent figures strongly indicate that sulfur which is produced by the electrocatalytic reaction [5], must also be consumed in a consecutive electrocatalytic step, *i.e.*

$$S + 2\,O^{2-} \rightarrow SO_2 + 4e^- \quad [6]$$

The dashed curves on Fig. 3 and in subsequent figures are obtained from a kinetic model discussed below which assumes that reaction [6] is the major source of SO_2 formation. However, the possibility that direct H_2S oxidation to SO_2, according to reaction [2], is also taking place to a lesser extent cannot be excluded on the basis of the present data. Also, one cannot exclude the possibility that reactions [5] and [6] consist of several elementary steps involving chemisorbed oxygen formation from O^{2-} and consumption by H_2S and S. This, however, is not a likely possibility in the strongly reducing anodic environment.

As shown in Fig. 3b, the dependence of cell voltage V_{CW} on current density is rather complex. This is to be expected, since several competing reactions take place at the anode. Taking into account that the cathodic cell reaction is the reduction of $O_2(g)$ to form O^{2-}, one computes that the standard total cell potentials corresponding to the anodic reactions [2], [5], and [6] are 0.761, 0.785, and 0.748V, respectively, at 730°C. Inspection of Fig. 3b shows that at low current densities ($M < 0.06$) the cell potential is considerably higher than the above values. This shows that in this region the dominant anodic reaction is

$$H_2 + O^{2-} \rightarrow H_2O + 2e^- \quad [7]$$

which corresponds to a standard open-circuit cell potential of 0.998V at this temperature.

When all H_2 present at the anode is consumed by reaction [7], reactions [5] and [6] dominate. At intermediate current densities ($0.06 < M < 0.12$), the cell voltage decreases quasilinearly with current, and the slope is near the total cell resistance at this temperature, indicating ohmic polarization. The nonlinear V_{CW} decrease at higher current densities is indicative of diffusion overpotential. However, it can be easily shown that gas phase mass-transfer limitations are totally absent at these relatively low current densities in this reactor configuration (9, 21). Consequently, the appearance of diffusion overpotential may be related to the slow transfer of H_2S to the three-phase boundaries which may be blocked by sulfur forming multilayer structures on the Pt surface (32). This is further supported by the hysteresis behavior shown in Fig. 4, which shows the problems encountered when operating the cell at low M values leading to sulfur formation over long periods of time. Curve (a) in Fig. 4 is obtained when decreasing the current from 4 mA to zero by increasing the external resistive load over a period of 4h. Subsequent decreases in the external resistive load leads to curve (b) which corresponds to significantly lower power output and indicates the appearance of diffusion overpotential. Subsequent combustion of the sulfur deposited on the catalyst electrode by gaseous oxygen does not restore the initial electrocatalytic activity. This indicates that excessive sulfur formation leads to irreversible losses in the exchange current density i_0. Postmortem examination of anodes treated under such conditions showed extensive sintering or even detachment of the electrode from the solid electrolyte. All these problems can be overcome by operating the fuel cell under high current density, *i.e.*, high M, conditions which as shown in subsequent figures eliminates sulfur formation and leads to quantitative H_2S conversion to SO_2.

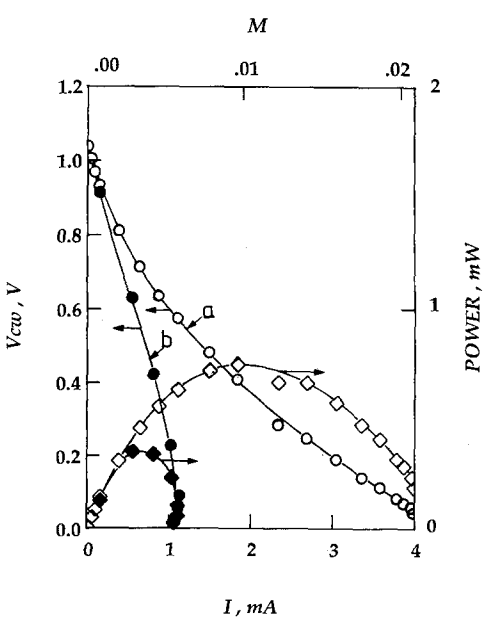

Fig. 4. Effect of current on cell voltage V_{CW} and power output for a fresh (curves a) and for a sulfur-poisoned (curves b) anode at low M values. G = 3.7 · 10⁻⁵ M/s, $y^{\circ}_{H_2S}$ = 0.89 · 10⁻², T = 653°C, reactor-cell 2. See text for discussion.

Typical current density at maximum power spontaneously generated by the cell is in this study of order 6 mA/cm² at 730°C (Fig. 3b). This is approximately a factor of 20 lower than that reported by Pujare *et al.* at 900°C using a $CuFe_2S_4$ anode (30). Much of this difference can be accounted for by the difference in electrolyte resistivity at these two temperatures and also to a lesser extent by the much higher anodic H_2S concentration used in reference (30). The existing data do not permit a direct comparison of the electrocatalytic activity of Pt and $CuFe_2S_4$ based on exchange current density values. Also, the product distribution of $CuFe_2S_4$ anodes is not yet known (30). From the open-circuit cell potential value (1.03V) and subsequent linear cell potential decrease with current presented in Ref. (30), it would appear that the cell was operated under conditions where H_2 oxidation was the dominant anodic reaction. Theoretical potentials given in Ref. (30) for reactions [5] and [6] are misleading, because apparently they were computed assuming that S(g) and not $S_2(g)$ is the dominant sulfur species present in the gas phase.

Figures 5 and 6 show typical results of the kinetic performance of the reactor cell over a wider range of oxygen-to-fuel ratios M, *i.e.*, $0 \leq M \leq 1.5$. In order to obtain M values near unity with the H_2S feed molar flow rates used (~10^{-7} moles H_2S/s) it was necessary to use the galvanostat. The main difference between Fig. 5 and 6 is in the feed molar flow rate. However, the behavior is similar when examined at the same M values. As shown in Fig. 5 and 6, when the ratio M exceeds the stoichiometric requirement of reaction [2], *i.e.*, $M > 0.33$, the selectivity to SO_2 exceeds 90% and approaches 100% for M values near unity where H_2S conversion also approaches 100%.

For M values exceeding unity, oxygen evolution was observed at the Pt catalyst electrode with only trace amounts of SO_3 formed.

At the transition between low and high selectivity, *i.e.*, near $M = 0.33$, rate and EMF oscillations were observed. This is a phenomenon frequently encountered in studies of Pt-catalyzed oxidations (9, 12). An example is shown in Fig. 7. The oscillations would typically disappear after a few hours of cell operation. This phenomenon has been observed also during regular catalytic H_2S oxidation on Pt and deserves further investigation, although it affects cell performance over a rather narrow range of conditions, *i.e.*, $0.3 < M < 0.4$.

Discussion

The ability of Pt to catalyze the oxidation of H_2S and S to SO_2 and SO_3 at temperatures above 300°C is well established in the catalytic literature (32-36). Hydrogen sulfide is known to chemisorb dissociatively on Pt and to form multilayer adsorbed sulfur "islands," which can further catalyze the chemisorption and oxidation of H_2S (32, 36). Sulfur oxidation to SO_2 and SO_3 is reasonably fast on Pt at temperatures above 300°C (32, 36) and appears to obey Langmuir-Hinshelwood kinetics (35, 36).

In view of the above information from the catalytic literature, it is not surprising that, as found in the present investigation, Pt is also a good electrocatalyst for the oxidation of H_2S to sulfur and to SO_2.

In order to describe the observed fuel cell kinetic behavior, one must take into account both the catalytic and electrocatalytic reactions taking place at the porous Pt anode. It should be noted that catalytic steps can take place over the entire Pt electrode surface area A, which is of order 300

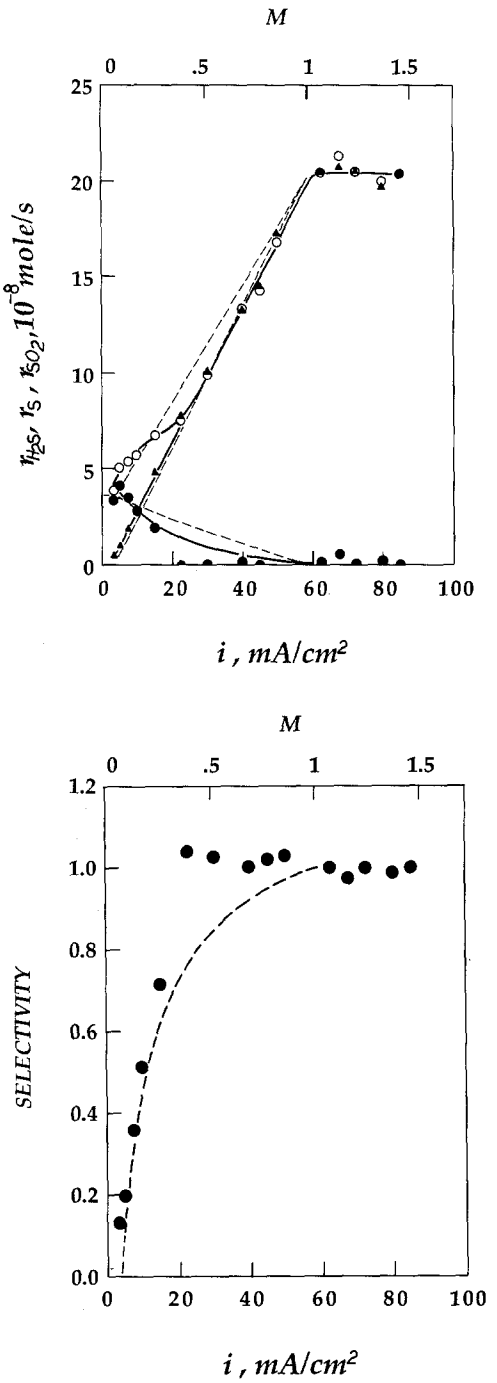

Fig. 5. (a, top) Effect of current density and M on r_{H_2S} (○), r_s (●), and r_{SO_2} (▲) at low inlet $y^\circ_{H_2S} = 0.47 \cdot 10^{-2}$, $G = 4.3 \cdot 10^{-5}$ M/s, $T = 700$°C, reactor-cell 3. Dashed lines from model, $\alpha = 0.10$. (b, bottom) Effect of current density and M on product selectivity to SO_2. Conditions as in Fig. 5a, dashed line from model, $\alpha = 0.10$.

cm² as determined on similar electrodes using surface titration techniques (12, 17). Electrocatalytic steps can only take place at the three phase boundaries between the zirconia electrolyte, the Pt electrode, and the gas phase. The latter does not exclude the possibility that some of the electrocatalytic action is taking place on F-centers on the zirconia surface as proposed by some workers (31), although practically all previous chemical cogeneration (22-29) or O^{2-} pumping studies (14, 15, 17-21), where quantitative product analysis was performed, have shown the product distribution to be electrode specific.

Model formulation.—Several models were examined in order to describe the kinetic behavior of the cell. The one presented below has the advantage that it is the simplest one which can describe the observed electrokinetic behavior in a semiquantitative manner. It contains only one parameter which was not measured independently. Other models examined contained up to three unknown parameters. They assumed Langmuir-Hinshelwood kinetics for the catalytic steps and also contained the electrocatalytic step [2]. These models had to be solved numerically, and although they contained up to three adjustable parameters, agreement with experiment was only marginally improved over the present one. The model proposed here can be solved analytically and provides a satisfactory fit to all the electrokinetic data, as shown by the dashed lines on Fig. 3-7.

The model considers that the entire Pt surface catalyzes the reaction

$$H_2S \xrightarrow{r} H_2 + S \qquad [3]$$

which is assumed first order in H_2S with a kinetic constant

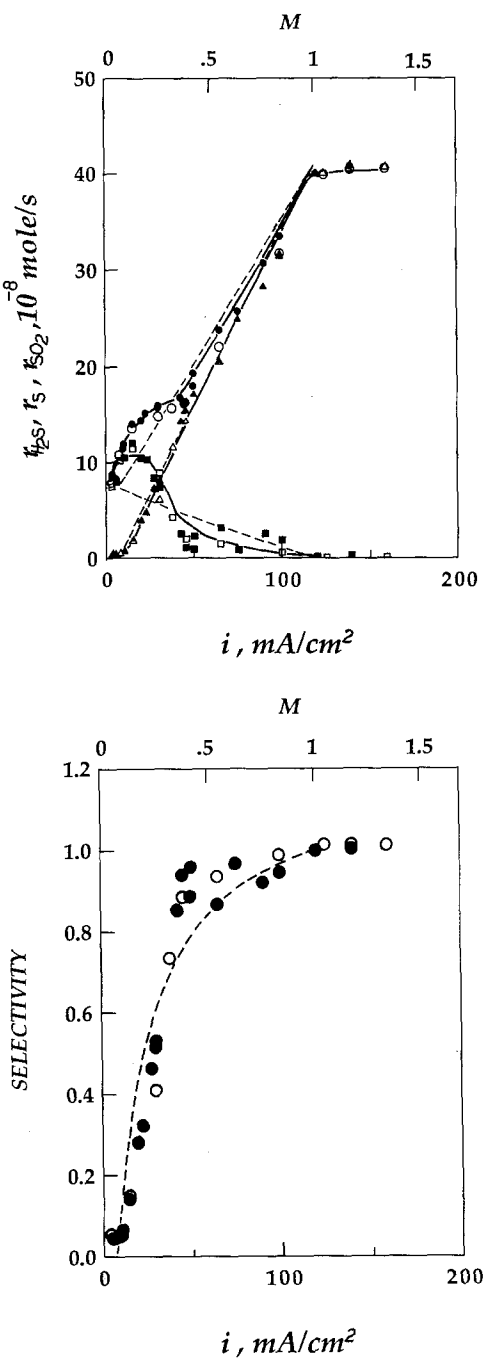

Fig. 6. (a, top) Effect of current density and M on r_{H_2S} (circles), r_s (squares), and r_{SO_2} (triangles) at high inlet $y^\circ_{H_2S} = 0.89 \cdot 10^{-2}$. Open symbols $T = 700$°C, filled symbols $T = 750$°C, $G = 4.6 \cdot 10^{-5}$ M/s, reactor-cell 3. Dashed lines from model, $\alpha = 0.10$. (b, bottom) Comparison of model predicted (dashed line, $\alpha = 0.10$) and experimental selectivity to SO_2. Conditions and symbols as in Fig. 6a.

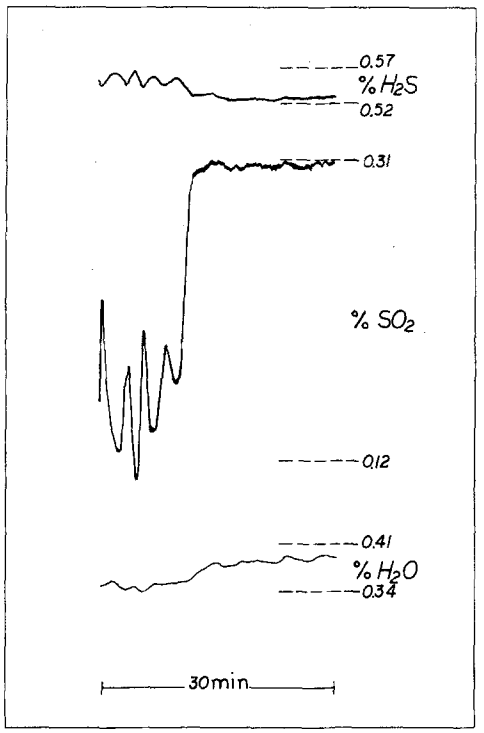

Fig. 7. Onset and disappearance of aperiodic rate oscillations. $y^\circ_{H_2S} = 0.89 \cdot 10^{-2}$, $G = 4.6 \cdot 10^{-5}$ M/s, $T = 750$°C, $i = 42$ mA/cm², reactor-cell 3.

k, *i.e.*, $r = kAy_{H_2S}$ where A is the surface area of the catalyst electrode and y_{H_2S} is the mole fraction of H_2S in the gas phase. The following electrocatalytic reactions are considered to take place at the three-phase boundaries

$$H_2 + O^{2-} \xrightarrow{I_1} H_2O + 2e^- \quad [7]$$

$$H_2S + O^{2-} \xrightarrow{I_2} S + H_2O + 2e^- \quad [5]$$

$$S + 2\,O^{2-} \xrightarrow{I_3} SO_2 + 4e^- \quad [6]$$

where $I = I_1 + I_2 + I_3$ is the total cell current. It is also assumed that reaction [7] is much faster than reactions [5] and [6] and that the ratio I_2/I_3 is proportional to the local concentrations of H_2S and S at the three phase boundaries, *i.e.*,

$$I_2/I_3 = \alpha y_{H_2S}/y_S \quad [8]$$

Equation [8] is, of course, an approximation of the model. It leads to significant mathematical simplification, since the anodic activation overpotential does not enter explicitly into the mass balance equations. One way to derive Eq. [8] rigorously is to assume (*i*) that reactions [5] and [6], which have similar standard potentials, are elementary reactions with equal anodic transfer coefficients, (*ii*) that H_2S and S chemisorption can be described by linear adsorption isotherms, and (*iii*) that the high field approximation of the Butler-Volmer equation is valid. Some of these assumptions may not be exactly valid, but the use of the approximate Eq. [8] in the model is justified by the resulting dramatic mathematical simplification and by the good agreement with experiment.

Taking into account that the anodic compartment of the fuel cell reactor used in this investigation is well-mixed (CSTR) over the range of flow rates used, one can write the following mass balances for the three components H_2S, S, and SO_2.

$$G(y^\circ_{H_2S} - y_{H_2S}) = kAy_{H_2S} + (I_2/2\mathbf{F}) \quad [9]$$

$$Gy_S = kAy_{H_2S} + (I_2/2\mathbf{F}) - (I_3/4\mathbf{F}) \quad [10]$$

$$Gy_{SO_2} = (I_3/4\mathbf{F}) \quad [11]$$

where G is the total anodic molar flow rate, $y^\circ_{H_2S}$ is the inlet H_2S mole fraction, and y_{H_2S}, y_S, and y_{SO_2} are the outlet H_2S, S, and SO_2 mole fractions, respectively. According to the model assumptions regarding the rates of the electrocatalytic reactions [5], [6], and [7], it is

$$I_1 = I,\ I_2 = I_3 = 0 \quad [12]$$

where $(I/2\mathbf{F}) \leq kAy_{H_2S}$, and

$$I_1 = 2\mathbf{F}kAy_{H_2S} \quad [13a]$$

$$I_2 = [\alpha y_{H_2S}/(y_S + \alpha y_{H_2S})]\,(I - 2\mathbf{F}kAy_{H_2S}) \quad [13b]$$

$$I_3 = [y_S/(y_S + \alpha y_{H_2S})]\,(I - 2\mathbf{F}kAy_{H_2S}) \quad [13c]$$

when $(I/2\mathbf{F}) \geq kAy_{H_2S}$. Introducing the dimensionless mole fractions $x_{H_2S} = y_{H_2S}/y^\circ_{H_2S}$, $x_S = y_S/y^\circ_{H_2S}$, $x_{SO_2} = y_{SO_2}/y^\circ_{H_2S}$ and the dimensionless parameters $N = kA/G$ and $M = I/6\mathbf{F}Gy^\circ_{H_2S}$, one can rewrite the model equations [9]-[11] in the form

$$1 - x_{H_2S} = Nx_{H_2S} + 3M(I_2/I) \quad [14a]$$

$$x_S = Nx_{H_2S} + 3M\{[I_2 - (I_3/2)]/I\} \quad [14b]$$

$$x_{SO_2} = 3M[(I_3/2)/I] \quad [14c]$$

In terms of these dimensionless quantities, the selectivity to SO_2 is defined from

$$s = x_{SO_2}/(1 - x_{H_2S}) \quad [15]$$

Model predictions and comparison with experiment.— Solution of Eq. [14a, b, c] for $I/2\mathbf{F} \leq kAy_{H_2S}$, *i.e.*, when Eq. [12] is valid, gives

$$x_{H_2S} = 1/(N + 1) \quad [16a]$$

$$x_S = N/(N + 1) \quad [16b]$$

$$x_{SO_2} = 0 \text{ and } s = 0 \quad [16c]$$

Equation [16] is valid when

$$M < \frac{N}{3(N + 1)} \quad [17a]$$

which ensures that $(I/2\mathbf{F}) \leq kAy_{H_2S}$. As an example for the conditions of Fig. 5 is $x_S = 0.18$, therefore $N = 0.22$. Consequently, the model predicts that for $M < 0.06$ the selectivity is zero, in reasonably good agreement with experiment. Under these conditions, oxygen anions O^{2-} react primarily with H_2 according to reaction [7].

When $I/2\mathbf{F} > kAy_{H_2S}$, or, equivalently

$$M > \frac{N}{3(N + 1)} \quad [17b]$$

the currents I_1, I_2, and I_3 are given from Eq. [13] and the model Eq. [14a, b, c] give

$$1 - x_{H_2S} = (Nx_{H_2S}x_S + 3M\alpha x_{H_2S})/(x_S + \alpha x_{H_2S}) \quad [19a]$$

$$x_S = (1/2)\,[3Nx_{H_2S}x_S + 3M(2\alpha x_{H_2S} - x_S)]/(x_S + \alpha x_{H_2S}) \quad [19b]$$

$$x_{SO_2} = (1/2)x_S\,(3M - Nx_{H_2S})/(x_S + \alpha x_{H_2S}) \quad [19c]$$

These equations can be reduced to a quadratic in x_{H_2S} with only one physically meaningful root and can be solved explicitly for x_{H_2S}, x_S, and x_{SO_2} in terms of the parameters M, N, and α. Then one can immediately compute the rates of H_2S consumption, and sulfur and SO_2 formation from

$$r_{H_2S} = Gy^\circ_{H_2S}(1 - x_{H_2S}) \quad [20]$$

$$r_S = Gy^\circ_{H_2S}x_S \quad [21]$$

$$r_{SO_2} = Gy^\circ_{H_2S}x_{SO_2} \quad [22]$$

and compare these rates with their experimental values. The N parameter value is easily computed from the open-

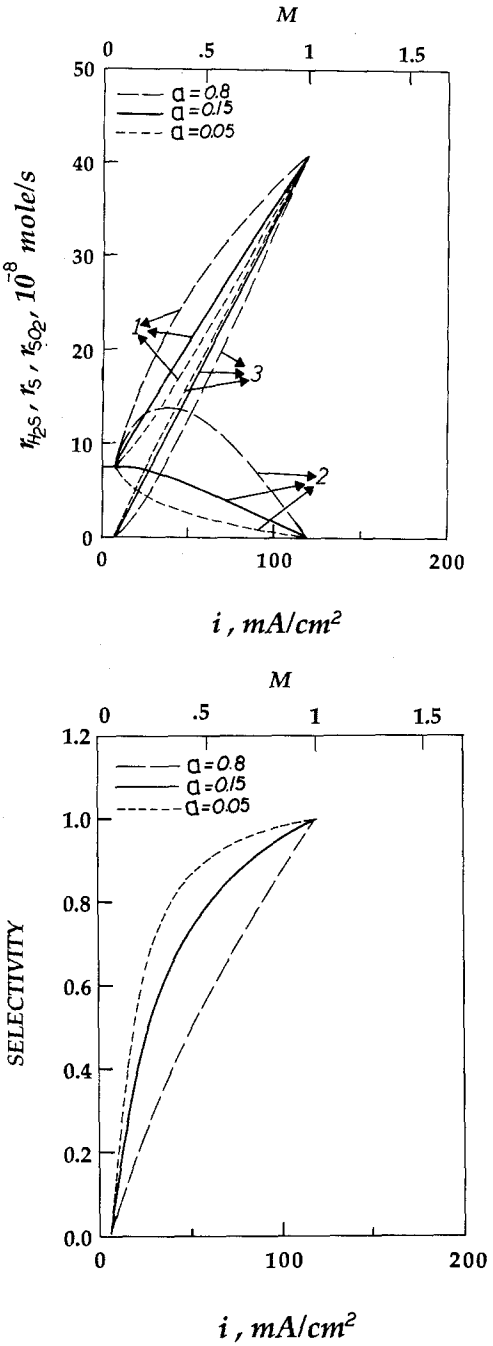

Fig. 8. Dependence of the model predictions for (a, top) reaction rates r_{H_2S} (1), r_S (2), and r_{SO_2} (3) and for (b, bottom) selectivity on the value of the exchange current-density ratio α. Conditions as in Fig. 6.

circuit H_2S conversion, *i.e.*, $N = (1 - x_{H_2S})/x_{H_2S}$, while M is a directly measured quantity. The only adjustable parameter is α. A least squares fit showed that $\alpha = 0.10$ provides a reasonably good fit to all the kinetic data over the range of temperatures and gaseous compositions studied. In Fig. 3, 5, 6, and 7, model predictions shown as dashed curves are compared with the experimental rate and selectivity data. It can be seen that agreement is quite satisfactory. The model correctly predicts that for $M = 1$ the selectivity and yield of SO_2 approach unity.

The agreement between model and experiment could be further improved by assuming that the parameter α is a function of overpotential and therefore a function of I and of M. This could eliminate the assumptions made to obtain Eq. [8]. Figure 8 shows the sensitivity of the model predictions to the value of α. Our kinetic results seem to indicate that α decreases with increasing M. Such a variation in α with M could also provide a means for explaining and modeling the observed rate and voltage oscillations. Further experimental and modeling work in this direction is currently underway. However, the model, even in its present simple form, is capable of describing all the essential experimental observations.

Conclusions

Hydrogen sulfide can be oxidized quantitatively to SO_2 in solid electrolyte cells with Pt electrodes operating in the temperature range 650°-800°C with simultaneous generation of electrical power. Product selectivity and power output performance of the cell depend crucially on the ratio M of the fluxes of O^{2-} and H_2S. Low M values lead to poor selectivity to SO_2, excessive sulfur formation, and concomitant deterioration of the cell power output characteristics. High (>0.33) M values lead to SO_2 formation and stable cell performance. A mathematical model has been developed which describes the kinetic behavior of the cell in a semiquantitative manner.

Acknowledgments

We thank the Stiftung Volkswagenwerk of Germany for financial support of this work through a Partnership Program Grant awarded to the Institut für Chemische Verfahrenstechnik of the University of Karlsruhe and to our Institute. We also thank Professor L. Riekert and Professor H.-G. Lintz of the above Institute for numerous helpful discussions and their student Mr. H. Hildebrand for grinding the thin solid electrolyte components. Financial support from the European Economic Community nonnuclear energy program is also gratefully acknowledged.

Manuscript submitted May 2, 1988; revised manuscript received Aug. 30, 1988.

REFERENCES

1. K. Denbigh, "The Principles of Chemical Equilibrium," 2nd ed., p. 76, Cambridge University Press, New York (1968).
2. J. A. Ketelaar, "Economic Evaluation of the Fuel Value for Fuel Cells," Sonderdruck aus Abhandlungen der Sächsissen Akademie der Wissenschaften zu Leipzig, Math.-Naturw. Klasse, Band 49, Heft 5, p. 289 (1968).
3. T. Weissbart and R. Ruka, *This Journal*, **109,** 723 (1962).
4. T. H. Etsell and S. N. Flengas, *ibid.*, **118,** 1890 (1971).
5. B. C. H. Steele, "Electrode Processes in Solid State Ionics," M. Kleitz and J. Dupuy, Editors, p. 367, Reidel-Dordrecht, Holland (1976).
6. E. C. Subbarao, "Solid Electrolytes and their Applications," Plenum Press, New York (1980).
7. A. O. Isenberg, *Solid State Ionics,* **314,** 431 (1981).
8. J. N. Michaels, C. G. Vayenas, and L. L. Hegedus, *This Journal,* **133,** 522 (1986).
9. C. G. Vayenas, B. Lee, and J. N. Michaels, *J. Catal.*, **66,** 36 (1980).
10. M. Stoukides and C. G. Vayenas, *ibid.*, **89,** 18 (1981).
11. M. Stoukides and C. G. Vayenas, *ibid.*, **82,** 45 (1983).
12. I. V. Yentekakis, S. Neophytides, and C. G. Vayenas, *ibid.*, **111,** 152 (1988).
13. R. Pancharatnam, R. A. Huggins, and D. M. Mason, *This Journal,* **122,** 869 (1975).
14. M. Stoukides and C. G. Vayenas, *J. Catal.,* **70,** 137 (1981).
15. M. Stoukides and C. G. Vayenas, *ACS Symp. Ser.*, **178,** 181 (1982).
16. T. M. Gür and R. A. Huggins, *J. Catal.*, **102,** 443 (1986).
17. I. V. Yentekakis and C. G. Vayenas, *ibid.*, **111,** 170 (1988).
18. C. G. Vayenas, *Proc. 6th Intl. Conf. Solid State Ionics,* Garmisch-Partenkirchen and Solid State Ionics, **28-30,** 1521 (1988).
19. C. G. Vayenas, S. Bebelis, and S. Neophytides, *J. Phys. Chem. Lett.*, **92,** 5083 (1988).
20. S. Bebelis and C. G. Vayenas, *J. Catal.* In press.
21. S. Neophytides and C. G. Vayenas, *ibid.*, (1989).
22. C. G. Vayenas and R. D. Farr, *Science,* **208,** 593 (1980).
23. R. D. Farr and C. G. Vayenas, *This Journal,* **127,** 1478 (1980).
24. C. Sigal and C. G. Vayenas, *Solid State Ionics,* **5,** 567 (1981).
25. J. N. Michaels and C. G. Vayenas, *J. Catal.*, **85,** 477 (1984).

26. J. N. Michaels and C. G. Vayenas, *This Journal*, **131**, 2544 (1984).
27. M. Manton, Ph.D. Thesis, Massachusetts Institute of Technology (1986).
28. N. Kiratzis and M. Stoukides, *This Journal*, **134**, 1925 (1987).
29. S. Neophytides and C. G. Vayenas, *ibid.*, Submitted.
30. N. U. Pujare, K. W. Semkow, and A. F. Sammells, *This Journal*, **134**, 2689 (1987).
31. B. G. Ong, T. A. Lin, and D. M. Mason, Abstract 531, p. 758, The Electrochemical Society Extended Abstracts, Vol. 87-1, Philadelphia, PA, May 10-15, 1987.
32. M. Steijns and P. Mars, *J. Catal.*, **35**, 11 (1974).
33. U. Köhler and H.-W. Wassmuth, *Surf. Sci.*, **117**, 668 (1982).
34. M.-V. Mathieu and M. Primet, *Appl. Catal.*, **9**, 361 (1984).
35. H. P. Bonzel and R. Ku, *J. Chem. Phys.*, **59**, 1641 (1973).
36. U. Köhler, M. Alavi and H.-W. Wassmuth, *Surf. Sci.*, **136**, 243 (1984).

Mass-Transfer Rate on a Plane Vertical Cathode with Hydrogen Gas Evolution

Y. Fukunaka, K. Suzuki, A. Ueda, and Y. Kondo

Department of Metallurgy, Kyoto University, Kyoto 606, Japan

ABSTRACT

Cathodic mass-transfer rate is enhanced by gas bubble evolution. In order to study this phenomena, a sectioned cathode, with insulation between each section, was used. The variations in mass-transfer coefficient, rising velocity of gas bubbles, and thickness of bubble dispersion layer in a vertical direction and due to current density were measured. The void fraction of the bubble dispersion layer was also obtained using these measurements. The measured ionic mass-transfer coefficient was analyzed by applying the additivity rule of micro- and macromixing proposed by Alkire and Lu. It was found that micromixing is caused by the convective flow of electrolyte during bubble growth on the cathode surface, and that the mass-transfer coefficient is proportional to the square root of the evolution rate of hydrogen gas bubbles. On the other hand, macromixing is caused by turbulent natural convection induced by the density difference between the electrolyte on the cathode surface in which hydrogen gas bubbles are dispersed and the bulk electrolyte. The measured mass-transfer coefficient due to macromixing expressed in terms of the Sherwood number was correlated to the Rayleigh number using the following expression

$$Sh_x = 1.72 \times 10^{-2} Ra_x^{1/2}$$

Electrolytic processes, in which gas bubble evolution occurs, offer many opportunities for interesting research. Two major effects of gas bubble evolution have been elucidated. One is the screening effect of growing gas bubbles which cover part of the surface area of the electrode. The ohmic resistance of electrolyte is also elevated by the presence of gas bubbles. Another effect is the enhancement of ionic mass-transfer rate to and from the electrode surface due to convective flow of electrolyte.

Tobias (1) studied the effect of gas-bubble evolution on the distributions of cathodic current density and the effect of the ohmic resistance of electrolyte. Stokes' law was applied to calculate the rising velocity of gas bubbles, and the volume fraction of gas bubbles in the electrolyte was obtained. Bruggenmann's equation was used to predict the variation of ohmic resistivity due to the volume fraction of gas bubbles. A notable effect of polarization on the leveling of nonuniformity of current density distribution was shown.

Several improvements were subsequently made, and the prediction of resistivity of electrolyte containing gas bubbles was improved. Hine *et al.* (2) measured the ohmic drop in dilute NaOH solution with a Luggin probe to find out the empirical equation of resistivity as a function of operational conditions and Barendrecht *et al.* (3) introduced the concept of a supercrowded bubble layer adjacent to the electrode surface. Recently, Ziegler and Evans (4) calculated the electrolyte velocity field and bubble distribution along 85 cm high insoluble lead anode immersed in $CdSO_4$ aqueous solution under the condition of electrowinning and compared them with measurements using a laser-Doppler velocimeter.

A number of electrochemical processes are controlled by ionic mass transfer. A typical example is the electrolytic production of sodium chlorate in which the rate of anodic discharge of hypochlorite ion is controlled by the ionic mass transfer. Beck (5) correlated the mass-transfer coefficient for anodic hypochlorite discharge with the anodic evolution rate of gas bubbles. He also noticed that the mass-transfer coefficients resulting from gas-bubble disengagement and from convective diffusion, two parallel processes, are additive.

The micromixing process of electrolyte on the electrode has been studied by many researchers. Ibl and Venczel (6) correlated the mass-transfer coefficient to the square root of the gas-bubble evolution rate. Janssen (7) studied the effect of bubble coalescence on the mass-transfer coefficient. A similarity to heat transfer in nucleate boiling was pointed out by Stephan and Vogt (8), and their model was compared with experimental data obtained by several researchers. More detailed analyses of the micromixing process on a micromosaic electrode (9) and the nucleation of hydrogen gas bubbles on a mercury pool electrode (10) have recently been reported.

In contrast, the number of studies on the ionic mass transfer due to macroscopic convective flow on the electrode is not so large. Ettel *et al.* (11) measured the mass-transfer coefficient of silver ion on a 1m high vertical electrode which was immersed in a $CuSO_4$-H_2SO_4 electrolyte for the purpose of optimization of the design of an electrowinning cell. Ionic mass transfer at a vertical gas-sparged electrode was studied by Sigrist *et al.* (12), and the Sherwood number was correlated with the Rayleigh number whose characteristic length was the bubble diameter. Alkire and Lu (13) followed Beck's proposal (5) and analyzed the dependence of mass-transfer coefficient on gas evolution rate and on the vertical distance along the cathode surface when immersed in an aqueous $CuSO_4$ solution acidified with sulfuric acid. For all their efforts, however, the characteristics of the macroscopic convective flow was not thoroughly clarified.

In the present paper, the technique proposed by Beck of dividing the mass-transfer coefficient into that due to micro- and macromixing components is employed. In addition, the role of macroscopic convective flow on the mass-transfer rate is pursued.

Experimental

Measurement of mass-transfer coefficient by anodic dissolution method.—The electrolyte cell was set up with acrylic resin plates and is shown in Fig. 1. The inner dimensions are 230 × 210 × 50 mm. The working sectioned electrode was composed of eight platinum sheets each of which is 20 × 20 × 0.1 mm in size. In order to keep the dis-